Relationship between the quantity of orexin receptor expression and calcium responses in cerebrocortical neurons:

An *in vivo* two-photon calcium imaging study with rhodamine-labeled orexin A

Saori Ohtani

Nihon University Graduate School of Dentistry

Major in Pharmacology

(Directors: Profs. Masayuki Kobayashi and Morio Tonogi,

and Assoc. Prof. Satoshi Fujita)

Index

This thesis is based on the following article and additional results in terms of oscillation of the calcium signal (Figs. 5 and 6C):

Ohtani S, Fujita S, Hasegawa K, Tsuda H, Tonogi M, Kobayashi M (2018) Relationship between the fluorescence intensity of rhodamine-labeled orexin A and the calcium responses in cortical neurons: An *in vivo* two-photon calcium imaging study. Journal of Pharmacological Sciences, 138: 76-82.

Abstract

Neural responses to a ligand vary widely between neurons; however, the mechanisms underlying this variation remain unclear. One possible mechanism is a variation in the quantity of receptor expression in each neural membrane. To examine this hypothesis, I synthesized a rhodamine-labeled orexin A compound, enabling us to quantify the amount of orexin binding to its receptors, OX_1 and OX_2, which principally couple to the $G_{q/11}$ protein. The rhodamine intensity and calcium response were measured from insular cortical glutamatergic neurons in *Thy1*-GCaMP6s transgenic mice under tetrodotoxin application using an *in vivo* two-photon microscope. Applying rhodamine-labeled orexin A (10 μM) to the cortical surface gradually and heterogeneously increased both the intensity of the rhodamine fluorescence and $[Ca^{2+}]_i$. Calcium responses started simultaneously with the increase in rhodamine-labeled orexin fluorescence and reached a plateau within several minutes. High- and low-responding neurons were classified based on the peak amplitude of the $[Ca^{2+}]_i$ increase. The rhodamine fluorescence intensity was larger in the high-responding neurons than the low-responding neurons. Preapplication of SB334867 and TCS-OX_2-29, OX_1 and OX_2 antagonists, respectively, decreased the proportion of high-responding neurons. These results suggest that the diverse receptor expression level in neural membranes is involved in mechanisms underlying varied neural responses, including $[Ca^{2+}]_i$ increases.

Introduction

The effects of G-protein-coupled receptor agonists show a wide variation at the cellular and synaptic levels. Previous studies have demonstrated the heterogeneous modulation profiles of the inhibitory postsynaptic currents (IPSCs) induced by adrenergic (Koyanagi et al., 2010) and cholinergic agonists (Yamamoto et al., 2010). The number of G-protein-coupled receptors expressed in neural membranes can change, e.g., by agonist-induced endocytosis (Tsao et al., 2001; Geppetti et al., 2015). Elucidating the effects of ligands in each neuron is one of keys to understanding the physiological function and developing research on the pathophysiology and treatment of nervous system diseases; however, little information is available about the relationship between the quantity of receptors and the degree of intracellular signaling in a living subject.

Orexin, also known as hypocretin, is involved in regulating wakefulness and appetite (de Lecea et al., 1998; Sakurai et al., 1998; Chemelli et al., 1999). Orexin receptor type-1 (OX_1) is coupled to the $G_{q/11}$ protein, whereas orexin receptor type-2 (OX_2) is coupled to multiple G-proteins, including $G_{q/11}$ and G_i (Zhu et al., 2003). Application of orexin increases intracellular Ca^{2+} concentration ($[Ca^{2+}]_i$; Sakurai et al., 1998; Zhu et al., 2003; Ozcan et al., 2010). Orexin also plays critical roles in diverse functions, such as reward, addiction, and pain (Baimel et al., 2015; Inutsuka et al., 2016; Peyron and Kilduff, 2017), which are partially processed in the insular cortex (IC; Jasmin et al., 2003; Nakamura et al., 2015; Kobayashi and Horinuki, 2017). IC receives projections of orexin-containing axons (Peyron et al., 1998; Date et al., 1999). Therefore, orexinergic receptors that are expressed in IC seem to be a suitable target for studying the relationship between the quantity of receptors and the $[Ca^{2+}]_i$.

In this study, I hypothesized that orexin heterogeneously regulates excitatory neurons in IC depending on a variation of the quantity of receptor expression in each neural membrane. To test this hypothesis, I synthesized rhodamine-labeled orexin A (Rhod-OX-A) and performed *in vivo* calcium imaging in *Thy1*-GCaMP6s transgenic mice expressing ultrasensitive fluorescent proteins as indicators of the $[Ca^{2+}]_i$ in a subpopulation of excitatory neurons. By using two-photon microscopy, I could visualize the $G_{q/11}$-dependent $[Ca^{2+}]_i$ increase by applying Rhod-OX-A in an *in vivo* preparation where the synaptic connections remained intact.

Materials and Methods

The Animal Experimentation Committee of Nihon University approved the experiments (AP17D003-1). Experiments were performed according to the institutional guidelines for the care and use of experimental animals described in the National Institutes of Health Guide for the Care and Use of Laboratory Animals. All efforts were made to minimize animal suffering and to reduce the number of animals used.

Synthesis of Rhod-OX-A

Almost all solvents and reagents were obtained from Nacalai Tesque (Kyoto, Japan), unless otherwise noted. Truncated orexin A (15-33) was synthesized starting from ChemMatrix resin (Sigma-Aldrich, St. Louis, USA) by solid-phase peptide synthesis with 9-fluorenyl-methyloxycarbonyl (Fmoc) amino acid derivatives (Peptide Institute, Osaka, Japan; Fig. 1A). After elongation of Arg(Pbf)-Leu-Tyr(tBu)-Glu(OtBu)-Leu-Leu-His(Trt)-Gly-Ala-Gly-Asn(Trt)-His(Trt)-Ala-Ala-Gly-Ile-Leu-Thr(tBu)-Leu, Fmoc-PEG2-Suc-OH (AnaSpec, Fremont, CA) was introduced to the N-terminus as a linker. After deprotection of Fmoc, the protected peptide resin was treated

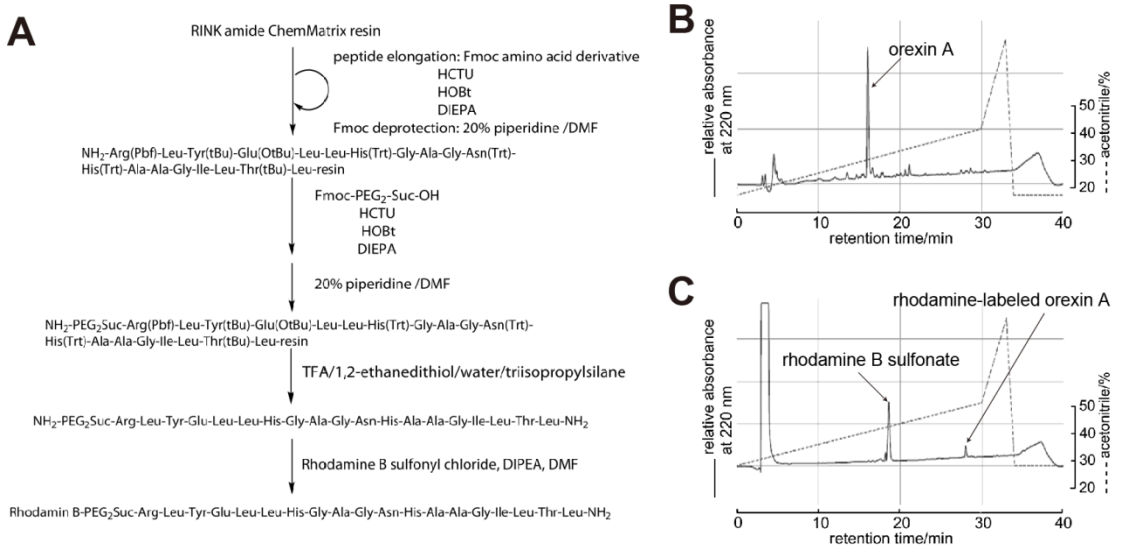

Figure 1. Synthesis of rhodamine-labeled orexin A (Rhod-OX-A). (A) Synthetic scheme of Rhod-OX-A. Truncated orexin A (15-33) was synthesized by a solid-phase peptide protocol with Fmoc-amino acid derivatives. After elongation, Fmoc-PEG2-Suc-OH was introduced as a linker, and Fmoc was deprotected with piperidine. The protected peptide resin was treated with a TFA cocktail for deprotection and cleavage. Truncated orexin A (15-33) was dissolved in DMF, and rhodamine B sulfonyl chloride was added to produce a rhodamine B conjugate. (B) HPLC profile of truncated orexin A (15-33). The arrow indicates the elution peak of truncated orexin A (15-33). (C) HPLC profile of Rhod-OX-A. The rhodamine B conjugation reaction was monitored with HPLC. After rhodamine B sulfonyl chloride was added, truncated orexin A (15-33) disappeared, and Rhod-OX-A was produced. A hydrolysate of rhodamine B sulfonyl chloride also appeared, which was marked as rhodamine B sulfonate. All compounds were confirmed by mass analysis.

with trifluoroacetic acid (TFA)/1,2-ethanedithiol/water/triisopropylsilane (88/5/5/2). The crude orexin A was loaded into a Sephadex G25 column (GE Healthcare) with 20% acetonitrile solution as the eluent at a flow rate of 1 ml/min. The orexin A fraction was collected and lyophilized as a white powder. Orexin A dissolved in *N*,*N*-dimethylformamide was added to Lissamine Rhodamine B sulfonyl chloride (Acros Organics, Geel, Belgium) and N,N-diisopropylethulamine. The Rhod-OX-A was purified with high-performance liquid chromatography (HPLC) using a Cosmosil $5C_{18}$-AR-II reversed-phase column (4.6 × 250 mm, flow rate 1.0 ml/min, gradient elution of water and acetonitrile containing 0.1% TFA solution; Fig. 1B, C) and obtained as a pink powder after lyophilization. The compound was measured by an Agilent 6130B electrospray ionization single quadrupole mass spectrometry (ESI-Q MS; Agilent, Santa Clara, USA).

Animal preparation

Transgenic GCaMP6s mice (C57BL/6J-Tg(*Thy1*-GCaMP6s)GP4.3Dkim/J, Jax #024275; Chen et al., 2013) aged over 7 weeks and weighing 25.4 ± 1.4 g (n = 14) were used. The mice received an injection of methylatropine bromide (5 mg/kg, i.p., European Pharmacopoeia Reference Standard) and were anesthetized with urethane (1.7 g/kg, i.p., Sigma-Aldrich). The body temperature was maintained at approximately 37 °C using a heating system (BWT-100, Bio Research Center, Osaka, Japan). To observe IC, mice were prepared according to previous studies with minor modifications (Fujita et al., 2016, 2017). Briefly, mice were fixed to a custom-made stereotaxic snout frame, which was tilted 90° laterally for imaging the left dorsal part of IC. After a subcutaneous injection of ropivacaine (AstraZeneca, Osaka, Japan), the temporal muscle and zygomatic arch were carefully removed. The skull was thinned to observe the middle cerebral artery (MCA) and rhinal fissure, which were used as landmarks to decide the location of craniotomy. A craniotomy (diameter = ~0.5 mm) was performed to expose the dorsal part of IC (Fig. 2A, B), and the dura matter was carefully resected.

In vivo *calcium imaging using two-photon microscopy*

The neurons in the transgenic GCaMP6s mice had fluorescent protein whose intensity increased depending on the $[Ca^{2+}]_i$ increase (Chen et al., 2013; Dana et al., 2014). Two-photon imaging was performed using a FVMPE-RS laser-scanning microscope system (Olympus, Tokyo, Japan) including a microscope (BX63, Olympus), a water-immersion objective lens (XLPLN25XWMP2; magnification = 25×, numerical aperture = 1.05, Olympus), and a pulsed laser (Insight DS Dual-OL, Spectra Physics, Santa Clara, USA). GCaMP6s was excited at 940 nm (Chen et al., 2013), and the emitted fluorescence was filtered through a bandpass filter (495-540 nm, Olympus). Rhod-OX-A was excited at 1040 nm, and the emitted fluorescence was filtered through a bandpass filter (575-645 nm, Olympus). Both wavelengths of the excitation laser were applied alternately at approximately 65 ms intervals, and the emitted fluorescence for each excitation wavelength was also alternately captured to avoid signal

contamination. Each acquired image was automatically averaged from 15 frames by the acquisition software (FV30S-SW, version 1.3.2.88, Olympus). The sampling intervals for the final stored data were 1.96 s. The imaging area was 255 × 255 μm^2 and consisted of 512 × 512 pixels.

Application of Rhod-OX-A

Calcium imaging was performed at a depth of 200 μm, corresponding to cortical layer II/III (Fig. 2Ca). Before application of Rhod-OX-A, 1 μM tetrodotoxin (TTX; Abcam, Cambridge, UK) was applied to the cortical surface to suppress spontaneous neural firing (Fig. 2Cb, c). In the experiment with antagonist application, 10 μM SB334867 (Tocris Bioscience, Abingdon, UK), an OX_1 antagonist, and 10 μM TCS-OX_2-29 (Abcam), an OX_2 antagonist, were applied simultaneously with TTX. After acquisition of the baseline, 10 μM Rhod-OX-A was applied to the cortical surface, and the calcium response of each neuron was recorded.

Anatomy

The observed regions were marked by an electrical current via a tungsten electrode. Then, the mice were deeply anesthetized with 5.0% isoflurane and perfused with saline through the ascending aorta, followed by 50 ml of a fixative containing 4% paraformaldehyde in 0.1 M phosphate buffer (PB, pH = 7.4). The brains were removed, postfixed overnight and cryoprotected in 30% sucrose in 0.1 M PB. The brains were frozen, sectioned coronally at 50 μm, and stained with 0.25% thionin to examine the recorded sites.

Data analysis

Calcium imaging data were processed and analyzed using software (Brain Vision Analyzer; Brainvision, Tokyo, Japan). Changes in the fluorescence intensity (ΔF) of each pixel relative to the initial fluorescence intensity (F) were calculated ($\Delta F/F$), and the ratio was processed with a spatial and a cubic filter. The region of interest (ROI) was set on each soma. I included data from neurons showing visually clear outlines (Fig. 3A, B). Neurons showing small and filled forms were considered as the edges of somata and were excluded from data to avoid contamination of neuropil signal due to limitation of resolution in Z-axis in two-photon microscopy. The shadow caused by thick vessels in the cortical surface often prevented clear outlines of the neurons; these data were excluded. Clear accumulation of rhodamine was found around vessels. To avoid contamination of high fluoresce due to the accumulation of Rhod-OX-A fluorescence in vessel cells (presumably astrocytes), I excluded data from the somata that were located adjacent to the blood vessels. To classify neurons as high- and low-responding neurons, the calcium signal of GCaMP6s was transformed to a Z-score using the following expression (Aoki et al., 2017).

$$\text{Z-score} = (fr_t - fr_0)/fr_{sds}$$

where fr_t is the $\Delta F/F$ for each frame, fr_0 is the $\Delta F/F$ just before the onset of the elevation in

rhodamine fluorescence, and fr_{sds} is the standard deviation (SD) of the $\Delta F/F$ value at baseline. Neurons in which the Z-score at the peak was greater than 5 were defined as high-responding neurons, and the remaining neurons were considered low-responding neurons.

To analyze the slow component of calcium oscillation, a moving average filter (-3 to 3 frames) was applied to the traces of fluorescent GCaMP6s 3 times. Then, the power spectral density was obtained using NeuroExplorer (ver. 4, Nex Technologies, Madison, USA). To compare the increase in the intensity of rhodamine fluorescence among different mice, the traces in high- and low-responding neurons were averaged in each mouse. And then, each pair of averaged traces was normalized to the maximum amplitude of rhodamine fluorescence in each mouse.

Statistics

For comparisons of the intensities between high- and low-responding neurons, unpaired *t* test following *F* test or the paired *t* test were appropriately used (Excel, version 2010, Microsoft, Redmond, USA). SigmaStat software (ver. 4.0, Systat Software, San Jose, USA) was used for comparison of the ratio of high-responding neurons between the conditions without and with OX_1/OX_2 antagonists, and $P < 0.05$ was considered significantly different. All data are expressed as mean ± SEM.

Results

Synthesis of Rhod-OX-A

Truncated orexin A (15-33) was synthesized successfully by a solid-phase method (Fig. 1B). However, rhodamine B sulfonyl chloride did not react with the N-terminus on the ChemMatrix resin. Therefore, the truncated orexin A (15-33) was cleaved from the resin, and rhodamine B sulfonyl chloride was conjugated by means of a solution-phase method. Finally, Rhod-OX-A was purified with HPLC (Fig. 1C). Rhod-OX-A was confirmed by ESI-Q MS ([M+H]+ Found: 2859.3, [M+H]+ Calcd: 2858.4).

In vivo *calcium imaging with and without TTX*

Thick vessels could be identified through the cranial bone, and a small window was opened caudal to the MCA (Fig. 2A). Then, calcium imaging was performed in IC (Fig. 2B). Fig. 2Ca shows a representative image, and neurons often showed a transient $[Ca^{2+}]_i$ increase (Fig. 2Cb). This Ca^{2+} transient was blocked by the application of 1 μM TTX to IC surface (Fig. 2Cc), suggesting that spontaneous action potentials induced the $[Ca^{2+}]_i$ increase. The amplitude and inter-event interval of $[Ca^{2+}]_i$ events were irregular and caused disruptions of observation. Therefore, 1 μM TTX was applied to inhibit spontaneous spike firing.

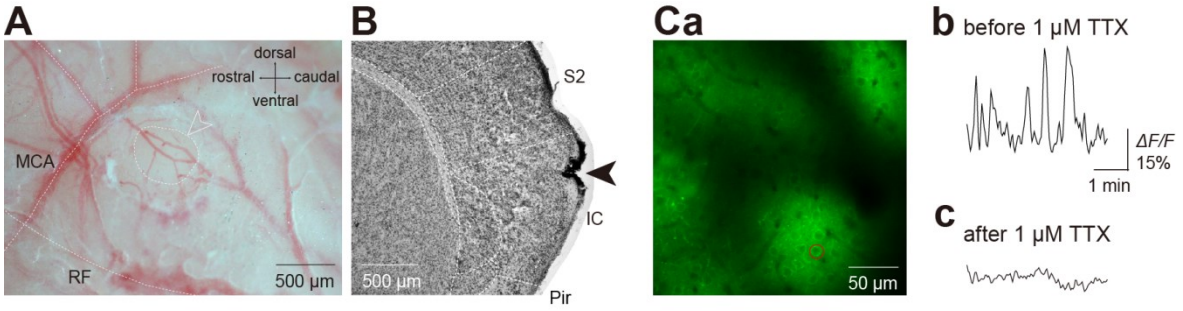

Figure 2. Calcium imaging of the dorsal part of insular cortex (IC). (A) An example of a craniotomy. The thinned skull enables us to observe the middle cerebral artery (MCA) and rhinal fissure (RF), which were used as landmarks to decide the location of craniotomy (diameter = ~0.5 mm). The outlined arrowhead and dashed circle indicate the area of craniotomy. (B) A coronal Nissl section showing the lesion of the observation area shown in (A). The craniotomy was performed on the dorsal part of IC. Filled arrowhead indicates the observed region which was marked by an electrode after the recording. (C) An example of field view (255 × 255 μm^2) consisting of 512 × 512 pixels (Ca) and traces of the calcium signal, as indicated by the intensity of GCaMP6s fluorescence, before (Cb) and after (Cc) the application of 1 μM tetrodotoxin (TTX). Note that the dark areas are due to thick vessels on the cortical surface. The neurons in the dark areas had unclear outlines and were excluded from the analysis. Traces were obtained from the neuron indicated by the red circle in (Ca). Pir, piriform cortex; S2, secondary somatosensory cortex

Application of Rhod-OX-A and calcium responses

After application of 10 μM Rhod-OX-A to IC surface, the intensity of rhodamine fluorescence

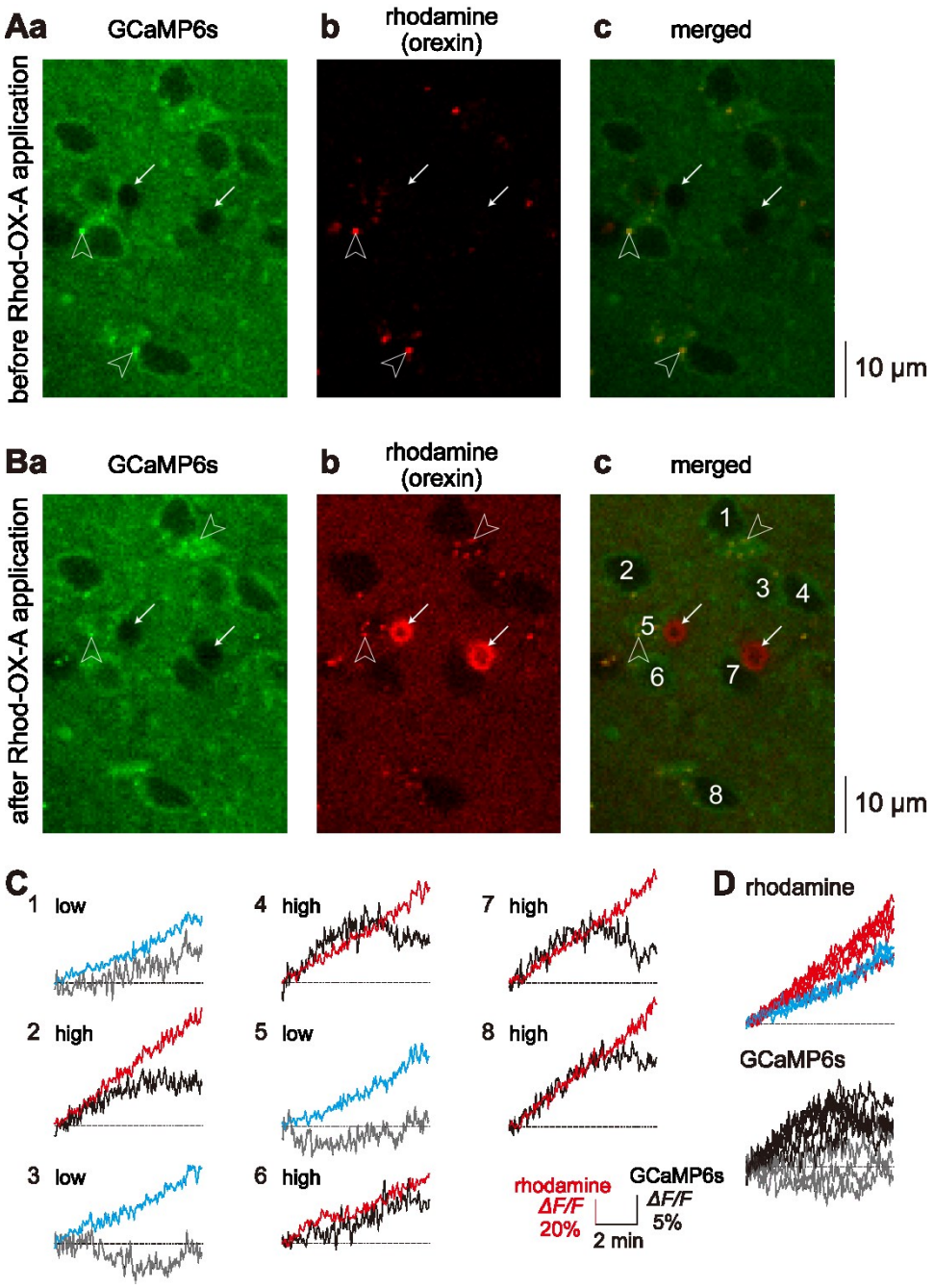

Figure 3. Representative responses to 10 μM Rhod-OX-A application. (A) GCaMP6s (Aa), rhodamine (Ab), and merged images (Ac) before Rhod-OX-A application. Note that several somata showed autofluorescence (arrowheads). (B) GCaMP6s (Ba), rhodamine (Bb), and merged images (Bc) after Rhod-OX-A application. Note that rhodamine was distributed in the whole area. Rhodamine accumulated around vessels (arrows). The granular mass that overlapped in the GCaMP6s and rhodamine images might be due to lipofuscin, which has autofluorescence (arrowheads). (C) Examples of calcium signals and rhodamine fluorescence after the application of Rhod-OX-A. The numbers correspond to those shown in (B). Red and blue lines indicate rhodamine fluorescence in high- and low-responding neurons, respectively. Black and grey lines indicate GCaMP6s fluorescence intensity in high- and low-responding neurons, respectively. Note that most of the neurons showed calcium responses that correlated with the increase in the rhodamine intensity. (D) The traces shown in (C) are superimposed. Note the heterogeneous amplitudes of rhodamine and $[Ca^{2+}]_i$.

gradually increased in whole area at the depth of 200 μm from IC surface (Fig. 3). The granular masses of fluorescence that overlapped in GCaMP6s and rhodamine images are presumably due to lipofuscin, which has autofluorescence (Fig. 3A, B; Schnell et al., 1999). On the other hand, a high accumulation of rhodamine fluorescence was observed around blood vessels (Fig. 3B, arrows), likely caused by nonneuronal cells.

The increase in rhodamine fluorescence is considered to involve two components: rhodamine binding to orexinergic receptors and unbound, passively diffusing rhodamine. Indeed, the increasing rates of rhodamine fluorescence varied from neuron to neuron (Fig. 3C, D), suggesting a variation in the orexinergic receptor expression. In parallel to an increase in the rhodamine fluorescence, the $[Ca^{2+}]_i$ was gradually increased in most of neurons (Fig. 3C), suggesting that the calcium responses were evoked by the Rhod-OX-A. However, the temporal pattern and the amplitude of the $[Ca^{2+}]_i$ increase were heterogeneous (Fig. 3D).

Comparison between high- and low-responding neurons

To quantify the relationship between $[Ca^{2+}]_i$ and the rhodamine fluorescence, imaged neurons were classified into two groups (see the Experimental Procedures): high- and low-responding neurons. I obtained 300 high-responding neurons and 141 low-responding neurons from 9 mice. The averaged peak amplitudes of GCaMP6s fluorescence were 10.45 ± 0.22% in high-responding neurons and 5.68 ± 0.22% in low-responding neurons.

The calcium signals in the high- (n = 35) and low-responding neurons (n = 20) obtained from the mouse shown in Fig. 3 were shown in Fig. 4A. Significant differences in the $[Ca^{2+}]_i$ between the high- and low-responding neurons were found approximately 1 min after the onset of the elevation in rhodamine fluorescence, and the difference became larger as time

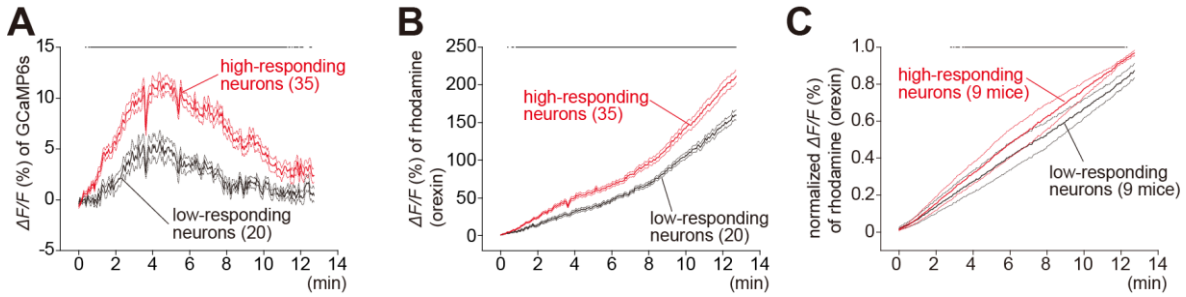

Figure 4. Higher rhodamine intensity in high-responding neurons than in low-responding neurons. (A) The mean (solid line) and SEMs (dashed lines) of calcium signals in the mouse corresponding to Fig. 3 were shown. High-responding neurons (Z-score of GCaMP6s fluorescence intensity > 5) showed higher calcium responses than did low-responding neurons. (B) The mean (solid line) and SEMs (dashed lines) of *ΔF/F* of rhodamine in the mouse corresponding to Fig. 3 were shown. The high-responding neurons showed a higher *ΔF/F* for rhodamine than did the low-responding neurons. (C) The mean (solid line) and SEMs (dashed lines) of normalized *ΔF/F* in rhodamine fluorescence obtained from 9 mice were shown. The range of significant differences in calcium signals (A) and *ΔF/F* of rhodamine (B), normalized *ΔF/F* (C) between high- and low-responding neurons are indicated by the horizontal lines at the top (*t* test).

advanced. Indeed, significant differences in rhodamine fluorescence intensity between the high- and low-responding neurons were observed from approximately 1 min after the rhodamine fluorescence began to increase (Fig. 4B).

To assess the rhodamine fluorescence in 9 mice, the averaged traces of high- and low-responding neurons were normalized and compared (Fig. 4C). The intensity of rhodamine fluorescence in the high-responding neurons was larger than that in the low-responding neurons from approximately 3 min.

Oscillation of the calcium signal

During the elevation of the calcium signal in response to the application of rhodamine-labeled orexin A, a slow oscillation was often observed (Fig. 5C). The power spectrum analysis revealed that the calcium signal involved a slow oscillation during the elevation in the calcium signals (Fig. 5D, arrowheads). The slow calcium oscillation peaked at 0.009, 0.019, and 0.042 Hz. The oscillation was also observed in the baseline (Fig. 5A), and the results of the power spectrum analysis showed peaks at similar frequencies (Fig. 5B). These results suggest that the slow oscillation in calcium responses independently occurred from the increase in the calcium signal.

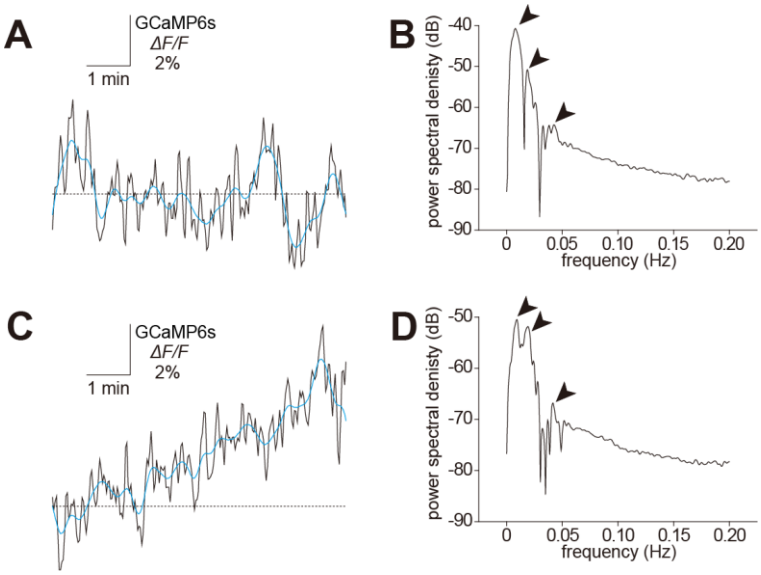

Figure 5. Slow calcium oscillation observed in IC neurons. (A) An example of the calcium signal at the baseline. The calcium signal (black line) was smoothed using a moving average filter (blue line). (B) Power spectral density profile of the smoothed trace in (A) shows peaks at 0.04-0.05 Hz and multiples thereof (arrowheads). (C) An example of a trace before (black line) and after (blue line) application of the moving average filter to the period of the increasing calcium signal. (D) Power spectral density profile of the smoothed trace in (C). Note that the slow oscillation was observed in both the increasing and stable periods.

Effects of OX_1 and OX_2 antagonists

To examine whether the Rhod-OX-A-induced calcium responses were mediated by orexin receptors, Rhod-OX-A was administered in the presence of a cocktail of OX_1 and OX_2 antagonists, SB334867 and TCS-OX_2-29, respectively (N = 5). Similarly to the application of Rhod-OX-A without antagonists, the rhodamine fluorescence gradually increased in the whole imaged area (Fig. 6A, B). The slow oscillation described above was also found during application of the orexinergic receptors antagonists (Fig. 6B, C). The granular mass around

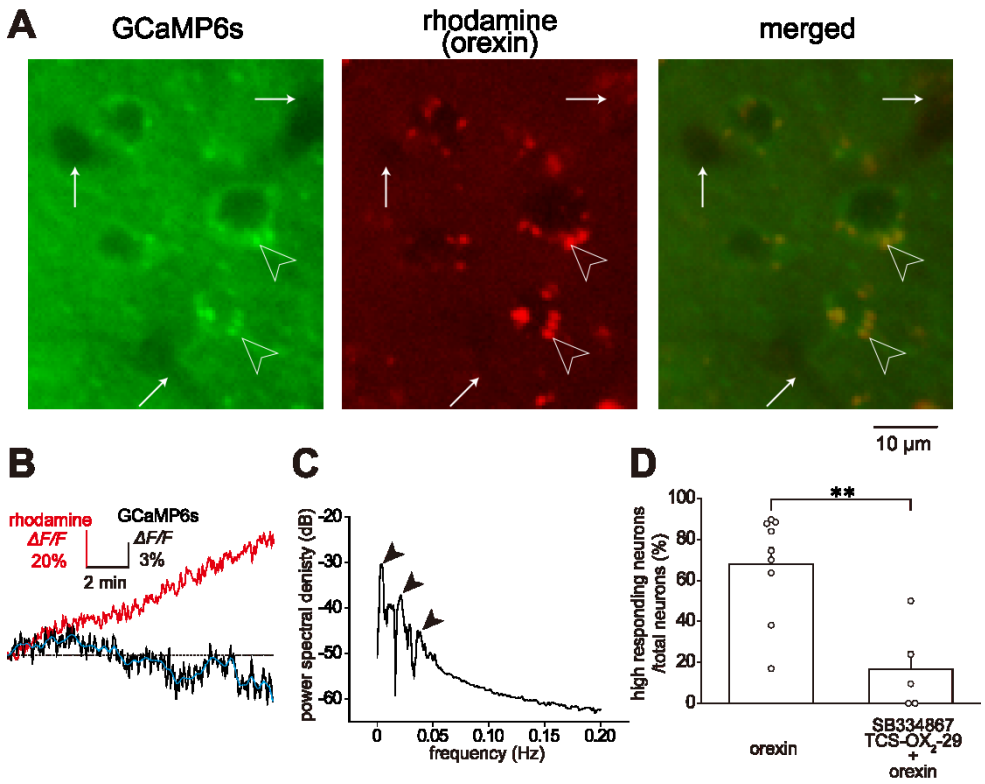

Figure 6. Calcium signals after Rhod-OX-A application with preapplication of the OX_1 and OX_2 antagonists. (A) An example of magnified GCaMP6s, rhodamine, and merged images. Note that rhodamine was distributed in the whole area in the presence of 10 μM SB334867, an OX_1 antagonist, and 10 μM TCS-OX_2-29, an OX_2 antagonist. An image of the granular masses that overlapped in the GCaMP6s and rhodamine images is shown. The accumulation of rhodamine around the vessels was unclear (arrows) compared to that without the OX_1 and OX_2 antagonists shown in Fig. 3. (B) An example of the traces for the calcium signal (black line) and the increased rhodamine fluorescence (red line) after the application of Rhod-OX-A. The trace for the calcium signal was smoothed using a moving average filter (blue line). (C) Power spectral density profile of the smoothed trace in (B) showing peaks at 0.04-0.05 Hz and multiples thereof (arrowheads). (D) Comparison of the ratio of high-responding neurons between the conditions without (n = 9) and with OX_1/OX_2 antagonists (n = 5). The preapplication of OX_1 and OX_2 antagonists significantly decreased the ratio (** $P < 0.01$, Student's t test).

some somata in GCaMP6s and rhodamine images overlapped under pre-application of antagonists (Fig. 6A, arrowheads); however, the accumulation of rhodamine around vessels was unclear (Fig. 6A, arrows) in comparison of the image without antagonists (Fig. 3B).

I analyzed the ratios of the 27 high-responding neurons and 170 low-responding neurons to the total neurons. Antagonist preapplication significantly decreased the averaged ratio of high-responding neurons from 68 ± 8% (N = 9) to 17 ± 8% (N = 5; $P = 0.0023$, Student's t test; Fig. 6D). These results show that the calcium responses that occur after the application of Rhod-OX-A are certainly mediated by orexin receptors.

Discussion

Calcium responses

Previous studies have reported that orexin application increases the $[Ca^{2+}]_i$ in cultured cells expressing orexin receptors (Sakurai et al., 1998; Zhu et al., 2003; Ozcan et al., 2010). The present experiment is in line with these studies and extended them by demonstrating the positive relationship between the fluorescence intensity of Rhod-OX-A and the $[Ca^{2+}]_i$ increase revealed by the GCaMP6s fluorescence in the *in vivo* preparation. The number of G-protein-coupled receptors expressed in the neural membrane is changed by agonist-induced endocytosis (Tsao et al., 2001; Geppetti et al., 2015). Thus, the diversity of calcium responses between high- and low-responding neurons could be explained by the quantity of receptors expressed in the neural membrane.

In a transgenic mouse expressing GCaMP6s under the *Thy1* promoter, GCaMP6s is expressed in a subpopulation of excitatory neurons (Sugino et al., 2006; Dana et al., 2014). Therefore, the difference in calcium responses in the present results is not due to a difference in neural types, e.g., excitatory vs. inhibitory neurons.

The calcium signaling evoked by activation of the $G_{q/11}$ protein involves several steps (Albrecht et al., 2001; Dickson et al., 2013). Activation of phospholipase C enzyme hydrolysis results in IP_3 and diacyl glycerol. IP_3 binds to IP_3 receptors on the endoplasmic reticulum, inducing calcium release from the endoplasmic reticulum. The released calcium further evokes calcium-induced calcium release via ryanodine receptors. If the expression level and/or their function of components of this pathway are different among neurons, the intracellular signaling could vary. Thus, the present results did not exclude the other possibilities that occur in the intracellular cascade.

Most neurons showed a decreased $[Ca^{2+}]_i$ after reaching the plateau in spite of an increase in the fluorescence intensity of Rhod-OX-A. This is possibly because of OX_1 internalization by β-arrestin as previously reported (Evans et al., 2001).

Rhod-OX-A

I synthesized Rhod-OX-A, which enables us to visualize the diffusion of orexin from the cortical surface toward a deep layer. Previous papers reported that two disulfide bonds in orexin A are not necessary for binding to the receptors and that a C-terminal sequence of 19 residues (15-33) can give a significant agonist effect (Darker et al., 2001; Takai et al., 2006). I referred to these papers to design a Rhod-OX-A with reduced molecular weight to improve the penetration rate. In addition, the introduction of polyethylene glycol as a hydrophilic linker decreased the hydrophobicity of the truncated orexin A (15-33). Although the Rhod-OX-A was distributed in the whole observation area, the outline of neurons was unclear compared to that in previous immunocytochemical images of OX_1 in the somatosensory cortex and frontal area 2 (Aracri et al., 2015). One possible reason for the discrepancy is that

the Rhod-OX-A that did not bind to receptors was not rinsed in this study: the unbound Rhod-OX-A increased the background fluorescence and made it difficult to observe the accumulation of Rhod-OX-A around the somata. The absorption in lipid-rich brain tissues would be attributed to the still high hydrophobicity of Rhod-OX-A. In addition, in contrast to the stable binding between an antigen and its antibody, Rhod-OX-A repeatedly binds to and dissociates from OX_1/OX_2. This unstable binding between the ligand and receptors would decrease the signal intensity.

Rhod-OX-A accumulated around vessels. Arteries, veins, and capillaries in the brain are sheathed by astrocytes (McCaslin et al., 2011; Boonstra et al., 2015). OX_1 and OX_2 express in cultured astrocytes in rats (Shu et al., 2014). Therefore, the accumulation may reflect binding of Rhod-OX-A to OX_1/OX_2 on perivascular astrocytes. This idea is supported by the results of the antagonist experiment (Fig. 6), in which the accumulation of rhodamine was unclear in the samples pretreated with antagonists.

Calcium oscillation

In this study, I applied TTX before the application of rhodamine-labeled orexin A, and the spontaneous firings were completely suppressed. However, a slow oscillation in the calcium signal was observed (Fig. 5). The power spectrum density profile revealed that the frequency had peaks at 0.04-0.05 Hz and multiples of this frequency. Therefore, the slow frequency was not due to cardiac or respiratory rhythms. It is reported that oscillatory hemodynamics of ~0.2 Hz is observed as Mayer waves in mice (Bumstead et al., 2017). However, the observed slow oscillation in the calcium signal was slower than that reported value. The present results suggest that IC neurons likely have an unknown intrinsic mechanism that generates a slow calcium oscillation.

Functional implications

IC plays a critical role in processing nociceptive information (Nakamura et al., 2015; Kaneko et al., 2017). IC is one of regions receiving projections from orexin-containing neurons (Peyron et al., 1998; Date et al., 1999). Several studies demonstrated an orexin-induced suppressive effect on nociception (Inutsuka et al., 2016, Razavi and Hosseinzadeh, 2017). I found that most IC excitatory neurons were sensitive to orexin A; however, the effectiveness of orexin A on calcium responses varied at the cellular level. The present findings suggest that IC neurons may process information, including nociception, depending on heterogeneous OX_1/OX_2 expression patterns. The differences in roles of OX_1 and OX_2 in IC should be investigated in future studies.

Acknowledgments

I am grateful to Prof. Masayuki Kobayashi and Assoc. Prof. Satoshi Fujita for their instructions of this study, Prof. Morio Tonogi for the opportunity to perform this study, and colleagues in Department of Pharmacology for their technical advice and assistance.

References

Albrecht MA, Colegrove SL, Hongpaisan J, Pivovarova NB, Andrews SB, Friel DD. (2001) Multiple modes of calcium-induced calcium release in sympathetic neurons I: attenuation of endoplasmic reticulum Ca^{2+} accumulation at low $[Ca^{2+}]_i$ during weak depolarization. J Gen Physiol. 118:83-100.

Aoki R, Kato R, Fujita S, Shimada J, Koshikawa N, Kobayashi M. (2017) Phase-dependent activity of neurons in the rostral part of the thalamic reticular nucleus with saccharin intake in a cue-guided lever-manipulation task. Brain Res. 1658:42-50.

Aracri P, Banfi D, Pasini ME, Amadeo A, Becchetti A. (2015) Hypocretin (orexin) regulates glutamate input to fast-spiking interneurons in layer V of the Fr2 region of the murine prefrontal cortex. Cereb Cortex. 25:1330-1347.

Baimel C, Bartlett SE, Chiou LC, Lawrence AJ, Muschamp JW, Patkar O, Tung LW, Borgland SL. (2015) Orexin/hypocretin role in reward: implications for opioid and other addictions. Br J Pharmacol. 172:334-348.

Boonstra E, de Kleijn R, Colzato LS, Alkemade A, Forstmann BU, Nieuwenhuis S. (2015) Neurotransmitters as food supplements: the effects of GABA on brain and behavior. Front Psychol. 6:1520.

Bumstead JR, Bauer AQ, Wright PW, Culver JP. (2017) Cerebral functional connectivity and Mayer waves in mice: Phenomena and separability. J Cereb Blood Flow Metab. 37:471-484.

Chemelli RM, Willie JT, Sinton CM, Elmquist JK, Scammell T, Lee C, Richardson JA, Williams SC, Xiong Y, Kisanuki Y, Fitch TE, Nakazato M, Hammer RE, Saper CB, Yanagisawa M. (1999) Narcolepsy in orexin knockout mice: molecular genetics of sleep regulation. Cell. 98:437-451.

Chen TW, Wardill TJ, Sun Y, Pulver SR, Renninger SL, Baohan A, Schreiter ER, Kerr RA, Orger MB, Jayaraman V, Looger LL, Svoboda K, Kim DS. (2013) Ultrasensitive fluorescent proteins for imaging neuronal activity. Nature. 499:295-300.

Dana H, Chen TW, Hu A, Shields BC, Guo C, Looger LL, Kim DS, Svoboda K. (2014) *Thy1*-GCaMP6 transgenic mice for neuronal population imaging *in vivo*. PLoS One. 9:e108697.

Darker JG, Porter RA, Eggleston DS, Smart D, Brough SJ, Sabido-David C, Jerman JC. (2001) Structure-activity analysis of truncated orexin-A analogues at the orexin-1 receptor. Bioorg Med Chem Lett. 11:737-740

Date Y, Ueta Y, Yamashita H, Yamaguchi H, Matsukura S, Kangawa K, Sakurai T, Yanagisawa M, Nakazato M. (1999) Orexins, orexigenic hypothalamic peptides, interact with autonomic, neuroendocrine and neuroregulatory systems. Proc Natl Acad Sci USA. 96:748-753.

de Lecea L, Kilduff TS, Peyron C, Gao X, Foye PE, Danielson PE, Fukuhara C, Battenberg

EL, Gautvik VT, Bartlett FS 2nd, Frankel WN, van den Pol AN, Bloom FE, Gautvik KM, Sutcliffe JG. (1998) The hypocretins: hypothalamus-specific peptides with neuroexcitatory activity. Proc Natl Acad Sci USA. 95:322-327.

Dickson EJ, Falkenburger BH, Hille B. (2013) Quantitative properties and receptor reserve of the IP_3 and calcium branch of G_q-coupled receptor signaling. J Gen Physiol. 141:521-535.

Evans NA, Groarke DA, Warrack J, Greenwood CJ, Dodgson K, Milligan G, Wilson S. (2001) Visualizing differences in ligand-induced beta-arrestin-GFP interactions and trafficking between three recently characterized G protein-coupled receptors. J Neurochem. 77:476-485.

Fujita S, Kaneko M, Nakamura H, Kobayashi M. (2017) Spatiotemporal profiles of proprioception processed by the masseter muscle spindles in rat cerebral cortex: an optical imaging study. Front Neural Circuits. 11:4.

Fujita S, Mizoguchi N, Aoki R, Cui Y, Koshikawa N, Kobayashi M. (2016) Cytoarchitecture-dependent decrease in propagation velocity of cortical spreading depression in the rat insular cortex revealed by optical imaging. Cereb Cortex. 26:1580-1589.

Geppetti P, Veldhuis NA, Lieu T, Bunnett NW. (2015) G protein-coupled receptors: Dynamic machines for signaling pain and itch. Neuron. 88:635-649.

Inutsuka A, Yamashita A, Chowdhury S, Nakai J, Ohkura M, Taguchi T, Yamanaka A. (2016) The integrative role of orexin/hypocretin neurons in nociceptive perception and analgesic regulation. Sci Rep. 6:29480.

Jasmin L, Rabkin SD, Granato A, Boudah A, Ohara PT. (2003) Analgesia and hyperalgesia from GABA-mediated modulation of the cerebral cortex. Nature. 424:316-320.

Kaneko M, Horinuki E, Shimizu N, Kobayashi M. (2017) Physiological profiles of cortical responses to mechanical stimulation of the tooth in the rat: An optical imaging study. Neuroscience. 358:170-180.

Kobayashi M, Horinuki E. (2017) Neural mechanisms of nociception during orthodontic treatment. J Oral Sci. 59:167-171.

Koyanagi Y, Yamamoto K, Oi Y, Koshikawa N, Kobayashi M. (2010) Presynaptic interneuron subtype- and age-dependent modulation of GABAergic synaptic transmission by beta-adrenoceptors in rat insular cortex. J Neurophysiol. 103:2876-2888.

McCaslin AF, Chen BR, Radosevich AJ, Cauli B, Hillman EM. (2011) In vivo 3D morphology of astrocyte-vasculature interactions in the somatosensory cortex: implications for neurovascular coupling. J Cereb Blood Flow Metab. 31:795-806.

Nakamura H, Kato R, Shirakawa T, Koshikawa N, Kobayashi M. (2015) Spatiotemporal profiles of dental pulp nociception in rat cerebral cortex: an optical imaging study. J Comp Neurol. 523:1162-1174.

Ozcan M, Ayar A, Serhatlioglu I, Alcin E, Sahin Z, Kelestimur H. (2010) Orexins activates protein kinase C-mediated Ca^{2+} signaling in isolated rat primary sensory neurons. Physiol

Res. 59:255-262.

Peyron C, Kilduff TS. (2017) Mapping the hypocretin/orexin neuronal system: An unexpectedly productive journey. J Neurosci. 37:2268-2272.

Peyron C, Tighe DK, van den Pol AN, de Lecea L, Heller HC, Sutcliffe JG, Kilduff TS. (1998) Neurons containing hypocretin (orexin) project to multiple neuronal systems. J Neurosci. 18:9996-10015.

Razavi BM, Hosseinzadeh H. (2017) A review of the role of orexin system in pain modulation. Biomed Pharmacother. 90:187-193.

Sakurai T, Amemiya A, Ishii M, Matsuzaki I, Chemelli RM, Tanaka H, Williams SC, Richardson JA, Kozlowski GP, Wilson S, Arch JR, Buckingham RE, Haynes AC, Carr SA, Annan RS, McNulty DE, Liu WS, Terrett JA, Elshourbagy NA, Bergsma DJ, Yanagisawa M. (1998) Orexins and orexin receptors: a family of hypothalamic neuropeptides and G protein-coupled receptors that regulate feeding behavior. Cell. 92:573-585.

Schnell SA, Staines WA, Wessendorf MW. (1999) Reduction of lipofuscin-like autofluorescence in fluorescently labeled tissue. J Histochem Cytochem. 47:719-730.

Shu Q, Hu ZL, Huang C, Yu XW, Fan H, Yang JW, Fang P, Ni L, Chen JG, Wang F. (2014) Orexin-A promotes cell migration in cultured rat astrocytes via Ca^{2+}-dependent PKCα and ERK1/2 signals. PLoS One. 9:e95259.

Sugino K, Hempel CM, Miller MN, Hattox AM, Shapiro P, Wu C, Huang ZJ, Nelson SB. (2006) Molecular taxonomy of major neuronal classes in the adult mouse forebrain. Nat Neurosci. 9:99-107.

Takai T, Takaya T, Nakano M, Akutsu H, Nakagawa A, Aimoto S, Nagai K, Ikegami T. (2006) Orexin-A is composed of a highly conserved C-terminal and a specific, hydrophilic N-terminal region, revealing the structural basis of specific recognition by the orexin-1 receptor. J Pept Sci. 12:443-454

Tsao P, Cao T, von Zastrow M. (2001) Role of endocytosis in mediating downregulation of G-protein-coupled receptors. Trends Pharmacol Sci. 22:91-96.

Yamamoto K, Koyanagi Y, Koshikawa N, Kobayashi M. (2010) Postsynaptic cell type-dependent cholinergic regulation of GABAergic synaptic transmission in rat insular cortex. J Neurophysiol. 104:1933-1945.

Zhu Y, Miwa Y, Yamanaka A, Yada T, Shibahara M, Abe Y, Sakurai T, Goto K. (2003) Orexin receptor type-1 couples exclusively to pertussis toxin-insensitive G-proteins, while orexin receptor type-2 couples to both pertussis toxin-sensitive and -insensitive G-proteins. J Pharmacol Sci. 92:259-266.